Picosecond laser writing of – 2 nanocomposite nanogratings for optical filtering

Maksim Sergeev, Yaroslava Andreeva, Vladislav Koval, Maxim Sergeev, Vadim P Veiko, Nathalie Destouches, Francis Vocanson, Hongfeng Ma, Anton Loshachenko, Tatiana Itina

Picosecond laser writing of $Ag - SiO_2$ nanocomposite nanogratings for optical filtering

Yaroslava Andreeva*[a], Vladislav Koval[a], Maxim Sergeev[a], Vadim P. Veiko[a], Nathalie Destouches[b], Francis Vocanson[b], Hongfeng Ma[b], Anton Loshachenko[c] and Tatiana E. Itina*[b,a]

[a] *ITMO University,Saint Petersburg 197101, Russia. E-mail: andreeva.ym@gmail.com*

[b] *Laboratoire Hubert Curien, UMR CNRS 5516/UJM-Saint-Etienne/Univ. Lyon, Saint-Etienne 42000, France. E-mail:tatiana.itina@univ-st-etienne.fr*

[c] *St Petersburg University, Saint Petersburg 199034, Russia*

Abstract

In this article, we propose a novel approach for fabricating of dielectric nanogratings via direct laser writing. Possibilities of a well-controlled ultrashort laser recording of Ag-SiO_2 nanocomposite gratings and their optical properties are examined. The mechanisms of laser processing involve silver nanoparticle growth in nanoporous silica glass films and laser interference-based formation of a periodic grating-like nanorelief. It is shown that laser energy should stay below a surface "grooves" formation threshold for laser-inscription of the interference-based grating. Otherwise, another periodic structure oriented parallel to the incident laser polarization appears to erase the interference pattern. The parameter windows required for a controlled fabrication of the obtained structures are determined. The required thresholds decay with the number of applied laser pulses is explained by a similarity in the roles of the absorbing nanoparticles and surface defect accumulation typically leading to such dependencies. The optical properties of the obtained gratings are shown to depend on the angle between the incidence plane and the grating direction. When these directions coincide, a signal enhancement with a period-dependent blue-shift is revealed in the diffuse scattering spectra. When these directions are perpendicular, the signal is less enhanced, and a red shift is observed. The observed results are promising in short laser fabrication of different optical components, such as, reflective optical filters.

Keywords: Laser surface structuring, laser fabrication, nanoparticles,

nanocomposites, silica glass

1. Introduction

Various surface patterns as well as micro- and nanostructures are traditionally of great practical interest in optics and photonics, where they are used for light manipulation , encoding and decoding optical information, for optical switching, interferometry, SERS, sensors, etc.[1, 2, 3, 4]. Additionally, the unique optical properties of the periodic surface structures, such as gratings and metasurfaces, further extend the range of their applications to security, chemistry, biology, and medicine [5].

Numerous studies focused on a surface nanostructures design and considerable progress was achieved [6, 7]. However, a well-controlled fabrication of such structures still represents a great challenge. For this, many methods were proposed ranging from bottom-up, such as colloidal and cluster chemistry [8], to top-down, including nanoparticle-assisted photo-lithography and multi-photon polymerization. However, nanoparticle manipulation at nanoscale and fabricating well-organized or periodic nanoparticle-containing structures are still challenging. In fact, many bottom-up procedures are particularly hard to control because of self-assembly or auto-organization that is often involved.

To solve this issue, a well-optimized laser treatment is particularly promising, namely because of the control possibilities that lasers can provide. In fact, lasers are known to be a powerful surface structuring tool [9] that can also be used for growing and tailoring the properties of nano-objects [10, 11], and, particularly, for nanoparticle formation in solid matrices [12].

Laser processing of transparent materials by beam interference further extended the possibilities of both surface and volume nanostructuring. In this case, additional possibilities related with nanoparticle presence [13, 14] and with laser beam focusing in the in bulk were explored [15]. The photo-controlled organization of metallic NPs in TiO_2 and SiO_2 films was also demonstrated [12]. Additionally, self-organized nanostructures were shown to be formed by scanning CW laser irradiation [16] and even femtosecond laser pulses [17].

Laser beam interference had already been shown to be promising for a controlled synthesis of silver nanoparticles (Ag NPs) in mesoporous TiO_2 films [18]. As a result, periodic structures consisting of highly ordered arrays of NPs were formed with period, comparable to laser wavelength. The

advantage of such 2D ordered nanoparticle arrays is in their sensitivity to the incident light, which depends on both the angle of incidence and the polarization direction [19, 20].

However, well-controlled synthesis of metallic NPs in nanostructures as well as laser modifications SiO_2 surface relief remain unstudied. In fact, the concentration of free electrons is very small in mesoporous SiO_2 matrices. These electrons are essential for the efficient ion reduction that allows nanocluster formation. As electron donors, polyatomic organic compounds or metallic salts can be used. For instance, a solution of silver nitrate in ethylene glycol was dissolved in such matrices [21, 22]. Upon laser irradiation, ethylene glycol is decomposed, so that free electrons are released and can be involved in the reduction of silver ions. It should be emphasized that the synthesis of Ag NPs in SiO_2 films becomes extremely difficult in the absence of such an electron donor.

This work aims to demonstrate the possibilities of a controlled synthesis of periodic structures in porous SiO_2 films prepared by the sol-gel method and impregnated with silver nitrate. For this, we use a laser beam interference set-up with two picosecond lasers operating in a scanning regime [23]. In the performed experiments, laser irradiation not only leads to silver nanoparticle formation and manipulation, but also to the periodic surface structuring of the nanocoposite films. The resulted periodic surface structures have several potential applications, namely as sensors, polarization splitters, couplers, etc. Additionally, such structures can be useful for molecular detection, photocatalysis [12, 24] as well as for diffracting deflector used in solar cells [25]. The revealed structure formation mechanisms are examined and explained. Finally, interesting optical properties of the obtained structures are discussed.

2. Materials and methods

2.1. Samples preparation

Mesoporous silica films were prepared following an evaporation induced self assembly (EISA) route as described in [26, 18]. Briefly, the sol-gel formulation was prepared by mixing tetraetoxysilane (TEOS) as silica precursor, with hydrochloric acid solution as catalyst, with tribloc copolymer F127 as structuring agent dissolved in ethanol. The films were deposited by dip-coating them on cleaned glass substrates before calcination at 673.15 K to remove the copolymer templates and form interconnected mesopores. Next, the films were soaked in an ionic silver nitrate solution 0.5 M (water/EtOH

1:1) for 1h before rinsing and drying at room temperature. The resulting film thickness is around 180 nm. The average pore size in the films is $\sim 7 \pm 3$ nm; the pore volume is $\sim$10%.

2.2. Laser treatment

An experimental setup used for laser micro processing by a two-beam interference field is shown in figure 1.

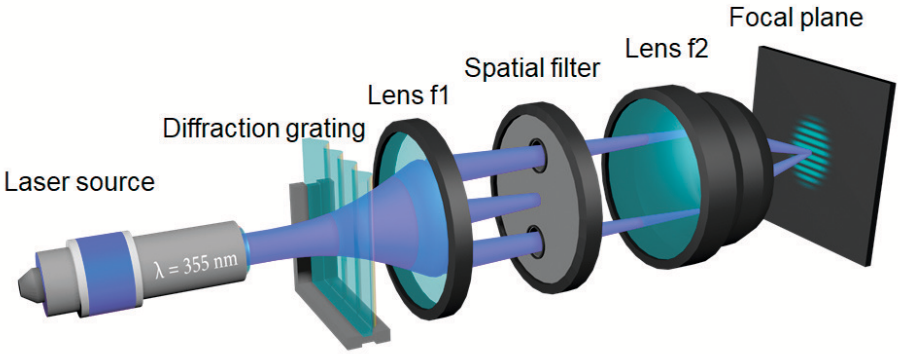

Figure 1: Experimental setup used for controlled laser writing of the two-beam interference patterns.

The processing schematics consists of a laser source, a block of mirrors, a phase diffraction grating with a period p=30 μm, a lens with a focal length f_1, a spatial filter, an aspherical lens with a focal length f_2, and a three-coordinate positioning system. Regarding the laser source, we used the third harmonic of picosecond Nd:YAG laser λ=355 nm at the repetition rate of f=10 Hz and a pulse duration equal to τ=30 ps. The average energy was varied from 3 to 60 μJ, and the number of pulses for one laser spot N was taken in the range from 1 to 1000. Optical transmission of the optical scheme was about 17%

To determine the modification threshold, laser processing was conducted in a stationary mode (without movements of the sample along X and Y axis). Taking into account the pulse repetition rate ν = 10 Hz and the

spot diameter d=98 μm, the scanning speed corresponding to this processing mode was determined as follows: V=$d\nu/N$.

To create a stable, double-beam interference pattern in the focal plane, a laser beam was split by a phase grating, and two identical beams of the first interference order were subtracted by a spatial filter. Next, the beams were focused by the second lens creating an interference pattern at the intersection [27, 28]. In the case of a confocal scheme, the angle between two beams is changed to manage the period of the pattern, which is determined as [29]:

$$\Lambda = \lambda/2sin\theta \tag{1}$$

where Λ is the period of the interference pattern, λ is the wavelength, θ is the angle between two beams. The angle θ is expressed through the distance between the diffraction maxima of $\pm$ 1 order and focal length f_2 as follows:

$$\theta = arctg(L_{\pm 1}/2f_2) \tag{2}$$

where $L_{\pm\ 1}$ is the distance between the diffraction maximums of $\pm$ 1 order and f_2 is a focal length of the second lens. Hence, the easiest way to change the angle between the interfering beams is to manipulate it with focal distance of the lenses. In our setup, the first lens was changed to obtain different periods of the interference field. To create interference patterns with the period of about 400 and 500 nm, we used lenses with focal distances of 8 and 9,7 mm, respectively. In both cases, the first micro lens with 300 mm focal distance was used. The expected (calculated) periods of nanostructures were 415 and 516 nm, but due to non-ideal optical scheme and optical losses on the components the actual nanopatterns with the periods of 410 and 540 nm occurred.

2.3. Characterization

To investigate the resulting structures on the nanoscale, a CrossBeam workstation Zeiss AURIGA as a scanning electron microscope (SEM) was used. The microscope has relatively high special resolution (images were carried out using SE2 detector at acceleration voltage 10-15 kV, beam current 600 pA) and good image contrast. Optical properties were characterized by using a microscope-spectrophotometer MSFU LOMO. The transmittance and reflectance spectra in visible wave range as well as diffusion reflectance spectra were measured in circular areas of about 50 μm in diameter. Carl Zeiss Axio Imager A1M optical microscope with the magnification up to

160× was used for visual analysis of the obtained structures in both reflected and transmitted light modes. The microscope is equipped with additional $\lambda/4$ plate allowing observations in the polarization contrast mode.

3. Results and discussion

3.1. Nanograting fabrication

The mesoporous SiO_2 thin films are activated by the presence of small Ag clusters and subjected to the scanning laser interference field. The direction of the interference pattern is parallel to the scanning direction. We use two identical laser beams and the absorption is enhanced by the formation and growth of silver nanoparticles (NPs). Consequently, different nanogratings were recorded at a constant scanning speed of V_{sc}=1.6 μm/s and various laser fluences. Figure 2 demonstrates SEM microimages of the nanogratings.

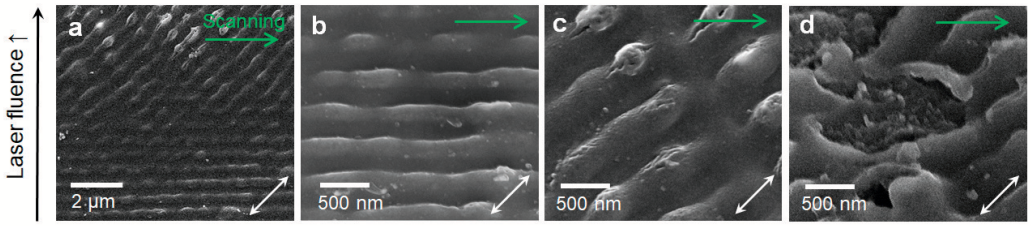

Figure 2: Nanograting formation. SEM image of the boundary zone and a schematics of radial distribution of laser energy (a). SEM images of the nanogratings with Λ_1=540 nm obtained for different laser fluences: interference pattern recorded at $F = 0.15$ J/cm^2 (b); urface grooves obtained at $F = 0.35$ J/cm^2 (c); destruction of the film occurred at $F = 0.68$ J/cm^2 (d). White double arrow corresponds to the polarization direction, the green arrow shows the scanning direction. Here, nanostructure depth varies with laser fluence, but does not exceed initial film depth.

The obtained nanostructures turned out to be oriented differently as a function of laser fluence. For lower laser fluences, structures are aligned along the scanning direction, as expected for the interference pattern (Fig.2b). With the increase in laser fluence, however, instead of the interference pattern based structure, another one appears and is oriented along laser polarization (Fig.2c). Further increase in laser fluence above a certain threshold obviously leads to film damage (Fig.2d).

An interference pattern is formed at smaller laser energy. With the increase in energy, the periodic structure appears to be parallel to laser polarization, contrary to our laser interference pattern. For instance, this effect can be observed in the central part of the laser track if peak laser fluence is too large. Such periodic self-organization is often observed in laser processing of various surfaces, including metals, semiconductors, dielectrics, ceramics, polymers, and nano-composites [30, 31, 32, 33, 34, 35, 36, 37]. Possible formation scenarios range from wave interference [30] to various instabilities and thermo-capillary waves [38]. The prevailing formation mechanisms depend on the laser-irradiated material, as well as on the fabricated structure orientation and periodicity. On one hand, periodic sub-wavelength structures, such as ripples, are typically formed at lower laser fluence and mostly oriented perpendicular to laser polarization. These small structures are attributed to the plasmonic effects [35, 39]. On the other hand, larger "grooves" are formed at higher fluences and are typically oriented parallel to laser polarization. These grooves are formed due to thermo-capillary waves, instabilities, or other thermodynamic phenomena [31].

To optimize the proposed laser processing technology, experiments were carried out revealing a strong dependency of the periodic structure orientation on laser fluence. In the experiments, we varied both the average laser energy E_0 and the number of laser pulses N from 1 to 1000. For structures with Λ=540 nm, E_0 was in the range from 3 to 60 μJ, and N varied from 1 to 1000.

To explain the obtained thresholds, formation mechanisms of the observed structures should be better understood. Figure 3 indicates the role of the applied pulses per laser spot. Even if laser repetition rate, laser spot diameter and nanoparticle concentration are small, several accumulation affects remain possible. Thus, nanoparticles are known to help enhancing electromagnetic field, promoting multi-photon ionization (MPI) and refractive index changes [40, 41]. More importantly, NPs serve as localized sources of electrons, ions and heat.

Nanoparticle heating process strats with electron energy absorption and electron-phonon relaxation in NP that takes up to several picoseconds, depending on nanoparticle material and size. The glass matrix is heated by the energy transfer from nanoparticles via convection and conduction, which typically takes up to several nanoseconds. Contrary to the heating, material cooling takes a longer, up to microseconds [42]. These processes are accompanied by a set of phase transitions, such as softening, densification,

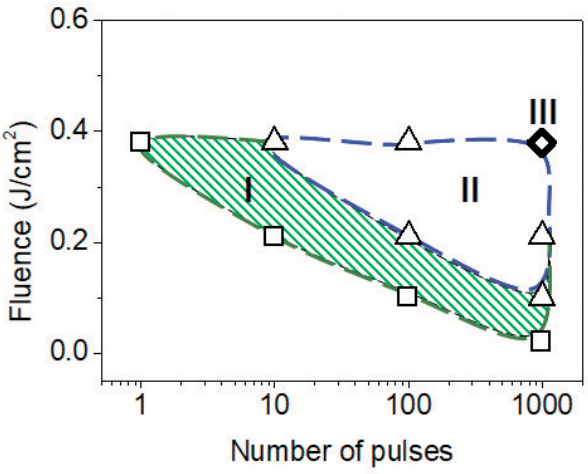

Figure 3: Laser processing regimes: zone I corresponds to the desirable interference pattern with Λ_1=540 nm recorded at F=0.15 J/cm^2 (Fig. 2b); zone II corresponds to the self-organized grooves (Fig. 2c); in the point 3, film destruction is observed (Fig. 2d).

.

crystallization, etc. [43]. These modifications also take a shorter time than the inter-pulse time in the present study (0.1 s).

In the case of fused silica, however, electrons can be also "stored" in self-trapped excitons [44, 45], considerably decreasing the material modification threshold in ultra-short multi-pulse irradiation regimes. In addition, surface relief and reflectivity/absorptivity changes are also accumulated [46, 47]. As a result, both structures' formation threshold's decay with N. Commonly, incubation and accumulation effects lead to the following pulse number dependency of the threshold fluence: $F = F_1 N^{S-1}$, where N is the number of laser pulses, F_1 is the single pulse threshold, and S is the slope. The results shown in Figure 3, line I, give $F_1 = 0.4\ J/cm^2$, and S is approximately $4e^{-5}$.

The periodic structures observed in the central part of the laser track (Fig. 2) better correspond to the grooves. For their formation, the laser-irradiated material should turn to a liquid state and its viscosity should typically reduce to allow convective liquid motion.

Thus, three observed thresholds (Figure 3) can be explained as follows:

(i) The formation threshold of the interference pattern should be connected to silica glass softening point at around T_1=1986 K.

(ii) For the grooves formation, glass should be heated up to the liquid

state and its viscosity, $\eta(T)$, should drop down, so the condition P_e>1 is satisfied, where P_e is Peclet number. This is known to take place at around T_2=3000 K [48].

(iii) The upper laser fluence limit is defined by the nanocomposite destruction that can be associated with boiling point, around T_3=3220 K.

Here we analyze the connections of laser processing parameters and optical properties via geometry of nanocomposite nanogratings. Furthermore, nanocomposite optical properties, are commonly calculated either based on Mie theory accounting for nanoparticle sizes and concentrations $\sum(\sigma_i \cdot n_i)$ [49, 50] or on a suitable effective medium approximation [51, 52], as will be shown below (Section 3.2).

3.2. Optical properties

The optical reflection R(λ) and transmission T(λ) of a periodic nanocomposite structure can be calculated as follows [53]:

$$R(\lambda) = \frac{\left[Re\sqrt{\epsilon_{full}(\lambda)} - \frac{1}{\sqrt{2}}\sqrt{\frac{1}{\cos^2\phi}}\right]^2 + \left[Im\sqrt{\epsilon_{full}(\lambda)}\right]^2}{\left[Re\sqrt{\epsilon_{eff}(\lambda)} - \frac{1}{\sqrt{2}}\sqrt{\frac{1}{\cos^2\phi}}\right]^2 + \left[Im\sqrt{\epsilon_{full}(\lambda)}\right]^2} \tag{3}$$

$$T(\lambda) = \frac{\left[1 - R_{eff}(\lambda)\right]^2 \exp\left(\frac{-4\pi}{\lambda}\frac{h}{\cos\phi}Im\sqrt{\epsilon_{full}(\lambda)}\right)}{1 - R_{eff}(\lambda)^2 \exp\left(-\frac{8\pi}{\lambda}\frac{h}{\cos\phi}Im\sqrt{\epsilon_{full}(\lambda)}\right)}, \tag{4}$$

where ϵ_{full} is the dielectric function of the effective medium, and ϕ is the angle between nanograting orientation and the direction of the incident light direction. The optical density of such materials is given by:

$$OD(\lambda) = \ln\left[1/T(\lambda)\right]. \tag{5}$$

More details about the calculation procedure can be found in the Appendix A.

The OD defines the total losses accounting for absorption, reflection, and scattering. Figure 4 shows the experimental and the calculated spectra of optical density. For both nanograting periods, a maximum near 430 nm is clearly observed. This maximum can be attributed to the surface plasmon resonance (SPR) of silver nanoparticles in the nanograting. The presence of the resonant NPs is also confirmed by SEM analysis (Fig. 5 b,c).

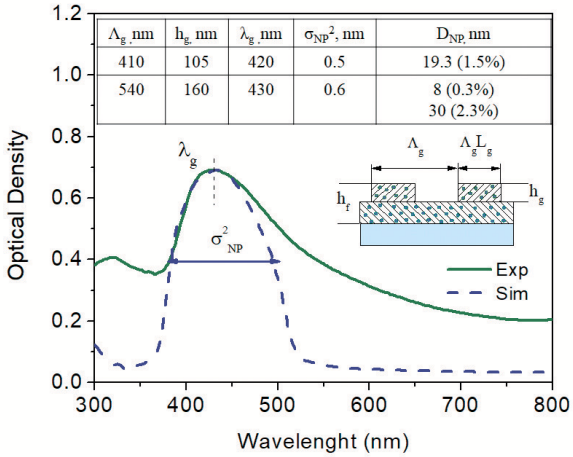

Figure 4: Measured and calculated optical density. Here, the incident light is normal to gratings surface. The inset and table show parameters used in the simulations.

Both peak position and width depend on the size, distribution, and volume fraction of the NPs. For our simulation, we determined NPs size and distribution by SEM, and the detailed data are presented in TableA.1 in the Appendix A). The volume fraction of the metallic phase, ν_{NP}, and NP's size dispersion, σ^2_{NP}, are determined and used in the additional simulation performed taking into account surface relief.

The optical properties of the fabricated nanostructures are then examined. For this, 1×1 mm regions were recorded without overlapping along the X axis. Scanning along Y-axis was performed for the revealed optimum laser irradiation conditions, that is at N=1000 and for F=0.21 and 0.33 J/cm^2 for Λ_1=410 nm and Λ_2=540 nm respectively.

The measured reflection spectra of the modified regions are presented in Figure 5. In the initial/non treated film, the reflection maximum is observed at 560 nm, which is typical for silver nanoparticle containing porous glass [54]. Upon the formation of the periodic structures on the surface, the peak is shifted. Interestingly, the shift strongly depends on the period of the formed structures: the maximum is observed at 480 nm for structures with periods $\Lambda_1 = 410$ nm, while for the ones with $\Lambda_2 = 540$ nm it is located at 530 nm. These shifts can be attributed to both laser-induced nanoparticles modifications and to the formation of the surface relief, as discussed below.

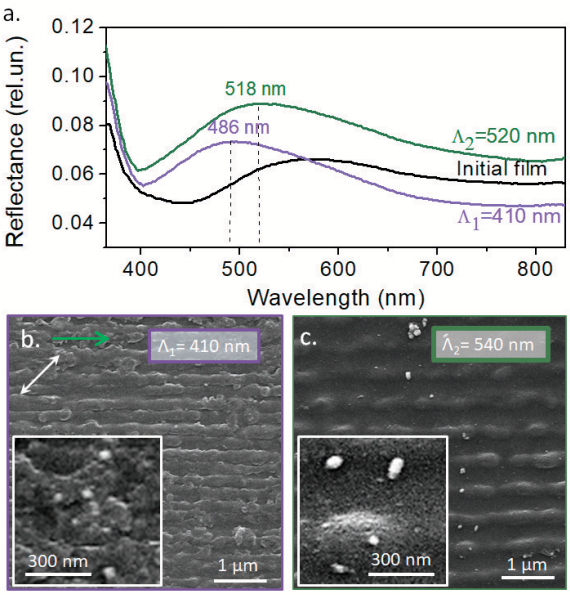

Figure 5: Reflectance spectra of the nanograings with different periods (a). SEM images of the nanogratings: structure with the period of $\Lambda_1 = 410$ nm obtained by laser scanning with the processing parameters N=1000, F=0.21 J/cm^2 (b), structure with the period of $\Lambda_2 = 540$ nm obtained by N=1000, F= 0.33 J/cm^2 (c). White double arrow shows the laser polarization direction, green arrow is a scanning direction

Additionally, Figure 6 (a) shows, furthermore, how the diffuse scattering spectra change for the incident angle of 45° and two different incident plane orientations: parallel and perpendicular to the grating direction. We emphasize that in both cases the created surface structures exhibit considerably different characteristics than the initial surface.

The diffuse scattering spectra reveal two distinctive peaks. The maximum positions depend on the period of nanograting and on the orientation of the incidence plane with respect to the periodic structures. For the direction parallel to the periodic surface structures, a significant increase in scattering is observed. The amount of the scattered light is much lower if the light incident plane is in the perpendicular direction.

The peaks observed near 402 and 498±1 nm for parallel direction correspond fairly well to the period of the nanograting $\Lambda_1 = 410$nm and $\Lambda_2 = 540$ nm. The scattering maximums observed for the orthogonal polarization direction are much less pronounced and exhibit slight red shift with the increase

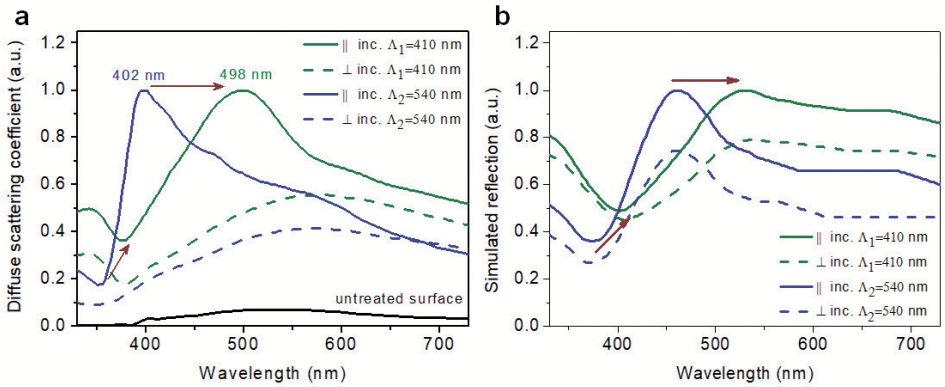

Figure 6: (a) Normalized experimental spectra of diffuse scattering of the gratings with $\Lambda_1 = 410$ nm and $\Lambda_2 = 540$ nm. (b) Simulated reflection spectra of the nanogratings.

of period. This peak can be explained by the Relay-Wood effect. The intensity and the position of this peak are related to the projection of the incident wave on the nanograting. Thus, the reflection of the resulting nanostructure is mostly in the range above 400 nm, and it can be controlled by rotating of the laser-induced surface structures.

Additionally, one can see a minimum around 350-400 nm corresponding to the plasmonic effect on the silver NPs in the dielectric matrix. The peak position does not depend on the illumination angle and slightly changes with a period of nanograting due to the differences in the NPs size and distribution. These results are confirmed by the simulation of the reflection presented in figure 6(b).

The described grating properties lead to an interesting visual effect, which can be observed in the crossed-polarized mode by using optical microscope (Figure B.7 in the Appendix B). The image acquires greater contrast while observed at angles of 0° and 90°, while at 45° the structure almost disappears.

4. Conclusion

To summarize, we have considered laser-based fabrication of a periodic gratin-like relief on the surface of a mesoporous silica film activated by the presence of silver nanoparticles using dual beam interference.

The obtained results demonstrate that the formation of the periodic structure strongly depends on laser fluence: in the case of lower laser fluence,

the grating formation correlates perfectly well with the beam interference pattern, whereas at larger laser fluence; periodic grooves are formed in the direction parallel to laser polarization. This second structure is attributed to thermo-hydrodynamic effects that erase the interference pattern in our experiments. At higher laser fluences, film damage is observed.

As a result of the performed experiments, a novel laser-based procedure of the controlled grating fabrication is proposed. Particularly, the fluence thresholds corresponding to both regimes have been shown to decay with the number of applied laser pulses indicating incubation and accumulation effects. This effect is attributed to electrons injected from nanoparticles as well as created by multi-photon ionization around nanoparticles, and stored in self-trapped excitons promoting structural changes and phase transitions. Surface reflectivity also changes in multi-pulse regimes.

Additionally, interesting optical properties of the interference-induced surface structures were revealed. This structure reflects mostly in the wavelength range above 400 nm, but differently when it is rotated parallel or perpendicularly to a light incident plane. Thus, it can be used for instance, as an optical filter and can be useful for second harmonic generation.

5. Acknowledgments

This research was performed in the frame of the PHC Kolmogorov France-Russia collaborative project Formalas operated by Campus France (38091TJ). ITMO Professorship and Fellowship program is gratefully acknowledged by TEI. H.M is grateful to The French Ministry of Science and Education for his PhD Scholarship.

SEM measurements were done on the base of Interdisciplinary Resource Centre for Nanotechnology, Research Park, St. Petersburg State University.

Appendix A. Calculation of the optical properties of diffraction gratings with Ag NPs

The obtained nanostructures were investigated both by SEM and optical spectrophotometry. The obtained experimental data was used in the modelling. Before and after laser irradiation, the average diameter, D_{av}, the relative concentration of NPs in composite C_{rNP}, and their dispersion σ_{NP2} were determined by SEM. Additionally, period Λ_g, depth h_g, and grating's coefficient L_g were also measured. The surface relief was then considered in the modeling of the grating's optical properties.

Firstly, the volume fraction ν_{NP} of all NPs and their concentrations were calculated. All the mentioned parameters are presented in Table A.1.

Properties	Ag-SiO_2 Film	Grating Λ_1	Grating Λ_2
average diameter D_{av}, nm	25	19.3	8/ 30
relative concentration C_{rNP}	0.019	0.074	0.066/0.019
concentration C_{NP}, Mol/m^3	0.218	0.028	0.036
dispersion ${\sigma_{NP}}^2$	0.7	0.5	0.6
volume fraction ν_{NP}	1.43	1.463	0.283/ 2.295
period Λ_g, nm	—	410	540
depth h_g, nm	180	105	160
grating's coefficient L_g	—	0.46	0.46

Table A.1: Properties of composite film before and after laser writing of nanogratings

Then, the effective dielectric function ε_{eff} of the nanocomposite $Ag - SiO_2$ film was determined. This function included the dielectric properties of metallic phase in the form of Ag NPs, and the matrix medium, namely the silica sol-gel porous film. The dielectric function of metallic phase, which depends on a wavelength of incident light, was described as the equation [55, 56]

$$\epsilon_{NP}(\lambda) = \epsilon_{Bulk}(\lambda) + s\frac{\lambda^2}{k^2\tau + ik\lambda} - z\Big[\frac{\lambda^2}{1 + ia\lambda} + \frac{\lambda^2}{1 + i(a+b)\lambda}\Big], \qquad \text{(A.1)}$$

where ε_{Bulk} - is the dielectric permeability of bulk material of NPs, τ=9.2 fs - time of electron relaxation.

The optical constants of silver were taken from [57]: ε_{Bulk}, $n = 5.86 \cdot 10^{28}$ is the free electron concentration, $m = 4.56 \cdot 10^{-31}$ kg is the effective mass of electron [57] with charge $e = 1.6 \cdot 10^{19}$ Kl, $\upsilon_F = 1.4 \cdot 10^6$ m/s is the Fermi velocity, $\varepsilon_0 = 8.85 \cdot 10^{-12}$ F/m is the dielectric constant, $c = 3 \cdot 10^8$ m/s is the light velocity in vacuum, $r_{NP} = 0.5D_{av}$ - radius of spherical particles, $\rho = 10500\ kg/m^3$ is the silver density, $N_A = 6.02 \cdot 10^{23}$ 1/Mol is the Avogadro constant, m_a=0.108 kg/Mol is the atomic mass of silver. The coefficients s, k, a and b were described by following equations:

$$s = \frac{4}{3}\frac{n_e^2 r_{NP}}{m\nu_F\epsilon}, k = 2, z = \frac{1}{12}\frac{N_A}{\epsilon_0 m_a m}\left(\frac{e}{\pi c}\right)^2, a = \frac{1}{2\pi^2 c\tau}, b = 0.75\frac{\nu_F}{2\pi c r_{NP}}, \tag{A.2}$$

where ε_{Bulk} is the dielectric permeability of bulk material of NPs, and τ=9.2 fs is electron relaxation time. The influence of transparent matrix on the optical properties of the metallic NPs was accounted for by using Bruggeman approximation with Bergman equation $\varepsilon_{eff} = f(\varepsilon_{NP}, \varepsilon_M, \nu_{NP}, \sigma_{NP})$ [58]. The dielectric permeability ε_M of sol-gel matrix SiO_2 was determined from optical constants of fused silica [53].

The surface relief in the shape of grating changed the optical properties of the composite film. To account for this, effective dielectric permeability should be corrected for composite layer with the thickness equal to h_g. New effective medium of this layer was determined as an average dielectric function between the composite and the environment by using the following shape function. The dielectric permeability of effective medium in the shape of the grating depended on grating orientation and on the incident light direction by using the the angel ψ between them. Finally, the dielectric permeability of grating in the air was determined as follows:

$$\varepsilon_g = \left\{ \left[1 + (\varepsilon_{eff} - 1)\,\nu_{gF}\right]^2 \cos^2\psi + \left[\frac{\varepsilon_{eff}}{\varepsilon_{eff} - (\varepsilon_{eff} - 1)\,\nu_{gF}}\right]^2 \sin^2\psi \right\}^{1/2}, \tag{A.3}$$

where ν_{gF} - is the volume fraction of grating as effective composite layer.

The total effective dielectric medium consists of two layers: the first of them with h_g thickness is the grating, the second layer with h_{film} - h_g thickness is the composite. The material of top layer was characterized by the

dielectric permeability ε_g, and the next layer under it by ε_{eff}. The effective dielectric permeability of the two-layer material was determined as:

$$\varepsilon_{full} = \frac{h_g}{h_{film}}\varepsilon_g + \left(1 - \frac{h_g}{h_{film}}\right)\varepsilon_{eff}. \tag{A.4}$$

Therefore, the optical reflection R(λ), transmission T(λ) and optical density OD(λ) of two-layers composite structure can be calculated using the equations 34.

After interaction with the grating, the reflected and transmitted lights were exposed to diffraction also known as Rayleigh-Wood effect [59]. As a result, the initiated light was split ed into the main maximum of 0 order and ± 1, $\pm 2 \ldots$ $\pm m$ orders. The diffraction efficiency of such grating for reflected and transmitted light with amplitude $\mathrm{A}_F = \mathrm{R}\bigvee\mathrm{T}$ for m diffracted order was determined as

$$\eta\left(m\right) = 4A_F^2 L_g^2 \cdot \mathrm{Sinc}^2\left(L_g m\right)\cos^2\left[2\left(\frac{\pi}{\lambda}h_g\right)^2\left(\sqrt{\varepsilon_{full}}\cos\varphi_t - \cos\varphi\right) + \frac{\pi}{2}m\right], \tag{A.5}$$

where φ_t - is the angel of refracted light. At the registration of reflected or transmitted light after it diffraction should be considered the sum intensity of all orders.

Based on the experimental data for the optical density of Ag-SiO_2 film and of the gratings (Λ_1=410 and Λ_2 = 540 nm), the optical spectra were simulated (fig. 5).

Based on the comparison between the simulated optical density with the experimental spectra, the average diameter D_{av}, concentration C_{NP} and volume fraction ν_{NP} were then corrected (Tab. A.1). The angel φ and its component φ_r were equal to 0. At this angel, the main maximum of diffracted light was propagated and the all orders m was equal 0.

After the correction of size and concentration of silver NPs, the spectra of diffused reflection at the angel of incident light $\varphi = 45^\circ$ were calculated by using equation A.5 (fig.6). The differences between the experimental and simulated spectra is caused by the imperfect grating shape. Thus, small variations of depth h_g and grating coefficient L_g caused fluctuations of the grating's optical properties.

Appendix B. Optical microimages of the obtained nanogratings

Figure B.7 demonstrates the structure with period of Λ_2 in the transmission mode with crossed polarizers as well as in phase-contrast reflection mode. It was found that the intensity of transmission varies depending on the angle of rotation of polarizers. The marginal region acquires greater contrast while observed at angles of 0° (fig.B.7a) and 90° (fig.B.7c) in crossed polarizers, while at 45° the structure almost disappears (Fig.B.7b). On the other hand, central region can be clearly seen under 45°. The differences in the pictures in this mode indicate anisotropy of the obtained area. It was shown that central region consists of the structures with the direction along the laser polarization, while the marginal region structures are orientated along the interference field. Thus the observed anisotropy is obviously related to the direction of the periodical structures.

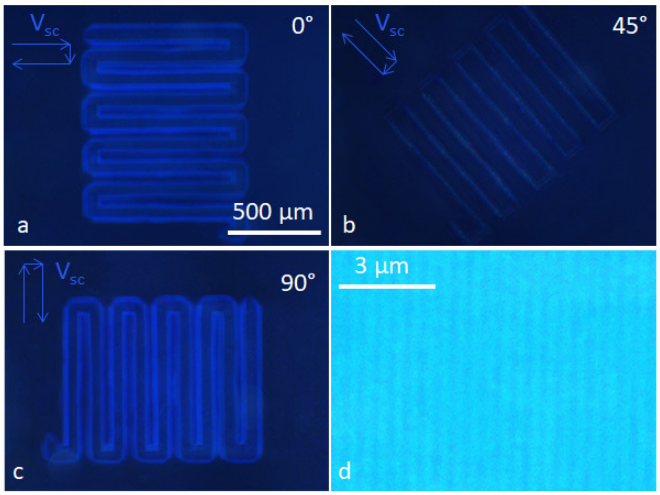

Figure B.7: Optical microimages of the structure obtained by laser scanning along Y-axis (F=0.33 J/cm^2, N=1000) under polarized light. The orientation of polarization vector is shown to be parallel or orthogonal to the orientation of the periodical structures. The sample is located at different directions: a initial direction; b sample rotated for 45°, c sample rotated for 90°. d phase-contrast microimage.

References

[1] D. Hülsenberg, A. Harnisch, A. Bismarck, Microstructuring of glasses, volume 87, Springer, 2008.

[2] M. Masuda, K. Sugioka, Y. Cheng, N. Aoki, M. Kawachi, K. Shihoyama, K. Toyoda, H. Helvajian, K. Midorikawa, 3-d microstructuring inside photosensitive glass by femtosecond laser excitation, Applied Physics A 76 (2003) 857–860.

[3] T. P. Otanicar, D. DeJarnette, Y. Hewakuruppu, R. A. Taylor, Filtering light with nanoparticles: a review of optically selective particles and applications, Advances in Optics and Photonics 8 (2016) 541–585.

[4] M. Gu, X. Li, Y. Cao, Optical storage arrays: a perspective for future big data storage, Light: Science & Applications 3 (2014) e177.

[5] C. L. Holloway, E. F. Kuester, J. A. Gordon, J. O'Hara, J. Booth, D. R. Smith, An overview of the theory and applications of metasurfaces: The two-dimensional equivalents of metamaterials, IEEE Antennas and Propagation Magazine 54 (2012) 10–35.

[6] R. Marqués, F. Martin, M. Sorolla, Metamaterials with negative parameters: theory, design, and microwave applications, volume 183, John Wiley & Sons, 2011.

[7] F. Bilotti, A. Toscano, L. Vegni, K. Aydin, K. B. Alici, E. Ozbay, Equivalent-circuit models for the design of metamaterials based on artificial magnetic inclusions, IEEE Transactions on Microwave Theory and Techniques 55 (2007) 2865–2873.

[8] R. M. Gazoni, M. G. Bellino, M. C. Fuertes, G. Giménez, G. J. Soler-Illia, M. L. M. Ricci, Designed nanoparticle–mesoporous multilayer nanocomposites as tunable plasmonic–photonic architectures for electromagnetic field enhancement, Journal of Materials Chemistry C 5 (2017) 3445–3455.

[9] M. Fukushima, H. Yanagi, S. Hayashi, H.-B. Sun, S. Kawata, Microfabrication of gold dots in sio2/tio2 glass films by two-photon absorption, Physica E: Low-dimensional Systems and Nanostructures 21 (2004) 456–459.

[10] B. Xu, W.-Q. Du, J.-W. Li, Y.-L. Hu, L. Yang, C.-C. Zhang, G.-Q. Li, Z.-X. Lao, J.-C. Ni, J.-R. Chu, et al., High efficiency integration of three-dimensional functional microdevices inside a microfluidic chip

by using femtosecond laser multifoci parallel microfabrication, Scientific reports 6 (2016) 19989.

[11] L. Jonušauskas, M. Lau, P. Gruber, B. Gökce, S. Barcikowski, M. Malinauskas, A. Ovsianikov, Plasmon assisted 3d microstructuring of gold nanoparticle-doped polymers, Nanotechnology 27 (2016) 154001.

[12] G. Baraldi, S. Bakhti, Z. Liu, S. Reynaud, Y. Lefkir, F. Vocanson, N. Destouches, Polarization-driven self-organization of silver nanoparticles in 1d and 2d subwavelength gratings for plasmonic photocatalysis, Nanotechnology 28 (2016) 035302.

[13] J.-Y. Natoli, L. Gallais, B. Bertussi, A. During, M. Commandré, J.-L. Rullier, F. Bonneau, P. Combis, Localized pulsed laser interaction with sub-micronic gold particles embedded in silica: a method for investigating laser damage initiation, Optics Express 11 (2003) 824–829.

[14] A. Podlipensky, A. Abdolvand, G. Seifert, H. Graener, Femtosecond laser assisted production of dichroitic 3d structures in composite glass containing ag nanoparticles, Applied Physics A 80 (2005) 1647–1652.

[15] S. Juodkazis, V. Mizeikis, H. Misawa, Three-dimensional microfabrication of materials by femtosecond lasers for photonics applications, Journal of Applied Physics 106 (2009) 8.

[16] Z. Liu, N. Destouches, G. Vitrant, Y. Lefkir, T. Epicier, F. Vocanson, S. Bakhti, Y. Fang, B. Bandyopadhyay, M. Ahmed, Understanding the growth mechanisms of ag nanoparticles controlled by plasmon-induced charge transfers in ag-tio2 films, The Journal of Physical Chemistry C 119 (2015) 9496–9505.

[17] Z. Liu, J. Siegel, M. Garcia-Lechuga, T. Epicier, Y. Lefkir, S. Reynaud, M. Bugnet, F. Vocanson, J. Solis, G. Vitrant, et al., Three-dimensional self-organization in nanocomposite layered systems by ultrafast laser pulses, ACS nano 11 (2017) 5031–5040.

[18] N. Destouches, Y. Battie, N. Crespo-Monteiro, F. Chassagneux, L. Bois, S. Bakhti, F. Vocanson, N. Toulhoat, N. Moncoffre, T. Epicier, Photodirected organization of silver nanoparticles in mesostructured silica and titania films, Journal of nanoparticle research 15 (2013) 1422.

[19] N. Destouches, N. Crespo-Monteiro, G. Vitrant, Y. Lefkir, S. Reynaud, T. Epicier, Y. Liu, F. Vocanson, F. Pigeon, Self-organized growth of metallic nanoparticles in a thin film under homogeneous and continuous-wave light excitation, Journal of Materials Chemistry C 2 (2014) 6256–6263.

[20] K. Loeschner, G. Seifert, A. Heilmann, Self-organized, gratinglike nanostructures in polymer films with embedded metal nanoparticles induced by femtosecond laser irradiation, Journal of Applied Physics 108 (2010) 073114.

[21] C. Luo, Y. Zhang, X. Zeng, Y. Zeng, Y. Wang, The role of poly (ethylene glycol) in the formation of silver nanoparticles, Journal of colloid and interface science 288 (2005) 444–448.

[22] P. Sudeep, P. V. Kamat, Photosensitized growth of silver nanoparticles under visible light irradiation: a mechanistic investigation, Chemistry of materials 17 (2005) 5404–5410.

[23] G. M. Burrow, T. K. Gaylord, Multi-beam interference advances and applications: nano-electronics, photonic crystals, metamaterials, subwavelength structures, optical trapping, and biomedical structures, Micromachines 2 (2011) 221–257.

[24] N. Crespo-Monteiro, A. Cazier, F. Vocanson, Y. Lefkir, S. Reynaud, J.-Y. Michalon, T. Kämpfe, N. Destouches, Y. Jourlin, Microstructuring of mesoporous titania films loaded with silver salts to enhance the photocatalytic degradation of methyl blue under visible light, Nanomaterials 7 (2017) 334.

[25] V. Gâté, L. Berthod, M. Langlet, F. Vocanson, I. Verrier, C. Veillas, A. Kaminski, O. Parriaux, Y. Jourlin, Dynamic interferometry lithography on a tio2 photoresist sol-gel for diffracting deflector module, Journal of Nanomaterials 2017 (2017).

[26] S. Bakhti, S. Biswas, C. Hubert, S. Reynaud, F. Vocanson, N. Destouches, Switchable silver nanostructures controlled with an atomic force microscope, The Journal of Physical Chemistry C 118 (2014) 7494–7500.

[27] V. Veiko, M. Yarchuk, R. Zakoldaev, M. Gedvilas, G. Račiukaitis, M. Kuzivanov, A. Baranov, Picosecond laser registration of interference pattern by oxidation of thin cr films, Applied Surface Science 404 (2017) 63–66.

[28] M. Gedvilas, B. Voisiat, S. Indrišiūnas, G. Račiukaitis, V. Veiko, R. Zakoldaev, D. Sinev, E. Shakhno, Thermo-chemical microstructuring of thin metal films using multi-beam interference by short (nano-& picosecond) laser pulses, Thin Solid Films 634 (2017) 134–140.

[29] G. Srikanth, Measurement of period of interference patterns with submicron period, Optics & Laser Technology 39 (2007) 918–921.

[30] M. Huang, F. Zhao, Y. Cheng, N. Xu, Z. Xu, Origin of laser-induced near-subwavelength ripples: interference between surface plasmons and incident laser, ACS nano 3 (2009) 4062–4070.

[31] G. D. Tsibidis, E. Skoulas, A. Papadopoulos, E. Stratakis, Convection roll-driven generation of supra-wavelength periodic surface structures on dielectrics upon irradiation with femtosecond pulsed lasers, Physical Review B 94 (2016) 081305.

[32] S. Gräf, C. Kunz, F. Müller, Formation and properties of laser-induced periodic surface structures on different glasses, Materials 10 (2017) 933.

[33] E. Golosov, V. I. Emelyanov, A. A. Ionin, Y. R. Kolobov, S. I. Kudryashov, A. E. Ligachev, Y. N. Novoselov, L. V. Seleznev, D. V. Sinitsyn, Femtosecond laser writing of subwave one-dimensional quasiperiodic nanostructures on a titanium surface, JETP letters 90 (2009) 107–110.

[34] S. Höhm, A. Rosenfeld, J. Krüger, J. Bonse, Laser-induced periodic surface structures on titanium upon single-and two-color femtosecond double-pulse irradiation, Optics express 23 (2015) 25959–25971.

[35] J. Bonse, A. Rosenfeld, J. Krüger, On the role of surface plasmon polaritons in the formation of laser-induced periodic surface structures upon irradiation of silicon by femtosecond-laser pulses, Journal of Applied Physics 106 (2009) 104910.

[36] J. Bonse, J. Krüger, S. Höhm, A. Rosenfeld, Femtosecond laser-induced periodic surface structures, Journal of Laser Applications 24 (2012) 042006.

[37] A. Rudenko, J.-P. Colombier, S. Höhm, A. Rosenfeld, J. Krüger, J. Bonse, T. E. Itina, Spontaneous periodic ordering on the surface and in the bulk of dielectrics irradiated by ultrafast laser: a shared electromagnetic origin, Scientific Reports 7 (2017) 12306.

[38] I. Ursu, I. Mihăilescu, A. Prokhorov, V. Konov, V. Tokarev, On the role of the periodical structures induced by powerful laser irradiation of metallic surfaces in the energy coupling process, Physica B+ C 132 (1985) 395–402.

[39] T.-Y. Derrien, R. Torres, T. Sarnet, M. Sentis, T. E. Itina, Formation of femtosecond laser induced surface structures on silicon: Insights from numerical modeling and single pulse experiments, Applied Surface Science 258 (2012) 9487–9490.

[40] A. Rudenko, J.-P. Colombier, T. E. Itina, From random inhomogeneities to periodic nanostructures induced in bulk silica by ultrashort laser, Physical Review B 93 (2016) 075427.

[41] G. Duchateau, Strong nonlinear electron multiplication without impact ionization in dielectric nanoparticles embedded in optical materials, Physics of Plasmas 20 (2013) 022306.

[42] V. P. Veiko, E. A. Shakhno, E. B. Yakovlev, Effective time of thermal effect of ultrashort laser pulses on dielectrics, Quantum Electronics 44 (2014) 322.

[43] D. Papazoglou, S. Tzortzakis, Physical mechanisms of fused silica restructuring and densification after femtosecond laser excitation, Optical Materials Express 1 (2011) 625–632.

[44] D. Ashkenasi, M. Lorenz, R. Stoian, A. Rosenfeld, Surface damage threshold and structuring of dielectrics using femtosecond laser pulses: the role of incubation, Applied Surface Science 150 (1999) 101–106.

[45] N. Itoh, A. M. Stoneham, Materials modification by electronic excitation, Radiation effects and defects in solids 155 (2001) 277–290.

[46] J. Bonse, J. Krüger, Pulse number dependence of laser-induced periodic surface structures for femtosecond laser irradiation of silicon, Journal of Applied Physics 108 (2010) 034903.

[47] I. Miyamoto, K. Cvecek, Y. Okamoto, M. Schmidt, H. Helvajian, Characteristics of laser absorption and welding in foturan glass by ultrashort laser pulses, Optics Express 19 (2011) 22961–22973.

[48] A. Rudenko, J.-P. Colombier, T. E. Itina, Nanopore-mediated ultrashort laser-induced formation and erasure of volume nanogratings in glass, Physical Chemistry Chemical Physics 20 (2018) 5887–5899.

[49] G. Mie, Beiträge zur optik trüber medien, speziell kolloidaler metallösungen, Annalen der physik 330 (1908) 377–445.

[50] S. Banerjee, D. Chakravorty, Optical absorption of composites of nanocrystalline silver prepared by electrodeposition, Applied physics letters 72 (1998) 1027–1029.

[51] L. A. Golovan, V. Y. Timoshenko, P. K. Kashkarov, Optical properties of porous-system-based nanocomposites, Physics-Uspekhi 50 (2007) 595.

[52] S. Srivastava, M. Haridas, J. Basu, Optical properties of polymer nanocomposites, Bulletin of Materials Science 31 (2008) 213–217.

[53] D. Smith, E. Shiles, M. Inokuti, The optical properties of metals, in: E. D. Palik (Ed.), Handbook of Optical Constants of Solids, Academic Press, Boston, 1985, pp. 369 – 406.

[54] L. De Boni, E. C. Barbano, T. A. de Assumpção, L. Misoguti, L. R. Kassab, S. C. Zilio, Femtosecond third-order nonlinear spectra of lead-germanium oxide glasses containing silver nanoparticles, Optics express 20 (2012) 6844–6850.

[55] J. Sancho-Parramon, Surface plasmon resonance broadening of metallic particles in the quasi-static approximation: a numerical study of size confinement and interparticle interaction effects, Nanotechnology 20 (2009) 235706.

[56] E. Cavaliere, G. Benetti, M. Van Bael, N. Winckelmans, S. Bals, L. Gavioli, Exploring the optical and morphological properties of ag and ag/tio2

nanocomposites grown by supersonic cluster beam deposition, Nanomaterials 7 (2017) 442.

[57] X. Zhang, Y. L. Chen, R.-S. Liu, D. P. Tsai, Plasmonic photocatalysis, Reports on Progress in Physics 76 (2013) 046401.

[58] J. Sturm, P. Grosse, W. Theiss, Effective dielectric functions of alkali halide composites and their spectral representation, Zeitschrift für Physik B Condensed Matter 83 (1991) 361–365.

[59] D. A. Pommet, M. Moharam, E. B. Grann, Limits of scalar diffraction theory for diffractive phase elements, JOSA A 11 (1994) 1827–1834.